CHEMISTRY
A EUROPEAN JOURNAL

DOI: 10.1002/chem.200601654

Selective Inclusion of Electron-Donating Molecules into Porphyrin Nanochannels Derived from the Self-Assembly of Saddle-Distorted, Protonated Porphyrins and Photoinduced Electron Transfer from Guest Molecules to Porphyrin Dications

Takahiko Kojima,*[a] Tatsuaki Nakanishi,[a] Ryosuke Harada,[b] Kei Ohkubo,[a] Seigo Yamauchi,[c] and Shunichi Fukuzumi*[a]

Abstract: A doubly protonated hydrochloride salt of a saddle-distorted dodecaphenylporphyrin (H_2DPP), $[H_4DPPP]Cl_2$, forms a porphyrin nanochannel (PNC). X-ray crystallography was used to determine the structure of the molecule, which revealed the inclusion of guest molecules within the PNC. Electron-donating molecules, such as *p*-hydroquinone and *p*-xylene, were selectively included within the PNC in sharp contrast to electron acceptors, such as the corresponding quinones, which were not encapsulated. This result indicates that the PNC can recognize the electronic character and steric hindrance of the guest molecules during the course of inclusion. ESR measurements (photoirradiation at $\lambda >$ 340 nm at room temperature) of the PNC that contains *p*-hydroquinone, catechol, and tetrafluorohydroquinone guest molecules gave well-resolved signals, which were assigned to cation radicals formed without deprotonation based on results from computer simulations of the ESR spectra and density functional theory (DFT) calculations. The radicals are derived from photoinduced electron transfer from the guest molecules to the singlet state of H_4DPP^{2+}. Transient absorption spectroscopy by femtosecond laser flash photolysis allowed us to observe the formation of $^1(H_4DPP^{2+})^*$, which is converted to $H_4DPP^{+\bullet}$ by electron transfer from the guest molecules to $^1(H_4DPP^{2+})^*$, followed by fast disproportionation of $H_4DPP^{+\bullet}$, and charge recombination to give diamagnetic species and the triplet excited state $^3(H_4DPP^{2+})^*$, respectively.

Keywords: crystal engineering · photochemistry · porphyrinoids · radical ions · self-assembly

[a] Prof. Dr. T. Kojima, T. Nakanishi, Dr. K. Ohkubo, Prof. Dr. S. Fukuzumi
Department of Material and Life Science
Graduate School of Engineering
Osaka University, SORST
Japan Science and Technology Agency (JST)
2-1 Yamada-oka, Suita
Osaka 565-0871 (Japan)
Fax: (+81) 6-6879-7370
E-mail: kojima@chem.eng.osaka-u.ac.jp
fukuzumi@chem.eng.osaka-u.ac.jp

[b] Dr. R. Harada
Center for Future Chemistry, Kyushu University
Moto-oka, Fukuoka 819-0395 (Japan)

[c] Prof. Dr. S. Yamauchi
Institute of Multidisciplinary Research for Advanced Materials
Tohoku University, Katahira, Sendai, Miyagi 980-8557 (Japan)

Supporting information for this article is available on the WWW under http://www.chemeurj.org/ or from the author. It contains crystallographic data (CIF format), elemental analysis data, the crystal structures of PNC–*p*-xylene and PNC–water, emission spectra of $[H_4DPP]Cl_2$, and electrochemical data for the hydroquinone derivatives and $[H_4DPP]Cl_2$.

Introduction

Photoexcitation of porphyrin compounds to give high-potential excited states results in photoinduced chemical and physical events both in vivo and in vitro.[1] For example, light-harvesting complexes in the photosynthetic systems of plants[2] and cyanobacteria are large aggregates of chlorophylls, which are Mg^{II}–porphyrin derivatives, to accumulate photon energy for energy and electron transfer. The energy transfer gives the excitation of the "special pair" in the reaction center,[3] from which electron transfer to plastoquinone B occurs to form the charge-separated (CS) state with a high potential ($\approx$1.1 eV).[4] Taking advantage of this high chemical potential, water splitting can proceed to give O_2 at the oxygen-evolving center of the tetranuclear manganese cluster by abstracting electrons from water.[5] The production of adenosine-5′-triphosphate (ATP) is also promoted by ATP synthase to obtain chemical energy for sustaining life.[6]

Porphyrin supramolecules have been prepared that model light-harvesting antenna complexes by self-assembly methods[7] and dendrimer constructions.[8] These molecules have been reported to exhibit effective energy transfer and electron migration. Another application for porphyrin-based supramolecules is the formation of CS states with high potentials by photoinduced electron transfer (PET).[9]

On the other hand, extensive efforts have been devoted to the development of photofunctional materials based on the self-assembly of porphyrin compounds. To date, a variety of porphyrin nanostructures have been reported, which includes nanorods that exhibit photoconductivity,[10] for the surface fabrication of electrodes towards the developments of photovoltaic cells.[11] Recently, Shelnutt and co-workers have developed a porphyrin nanotube that can form platinum nanoparticles on the surface to catalyze photochemical H_2 evolution.[12]

The self-assembly of porphyrin compounds has also attracted much attention in relation to the development of functional materials. One method is to construct porous materials with large channels that can encapsulate guest molecules in the channels with or without molecular recognition.[13] Molecular recognition over the course of guest encapsulation has been reported by Suslick and co-workers.[14] They have prepared zeolite-like porous materials through the self-assembly of metalloporphyrins and metal clusters, which demonstrated molecular recognition based on the shape and size of the guest molecules. However, porphyrin supramolecules that encapsulate guest molecules and show photofunctional capabilities have yet to be developed.

The construction of multicomponent supramolecular assemblies provides novel structures and integrated functionalities, which cannot be realized by each building block alone. We have developed novel porphyrin supramolecules by using dodecaphenylporphyrin (H_2DPP), which exhibits a saddle-distorted structure that can be recognized as a curved surface.[15] The use of H_2DPP as a ligand for a Mo^V center allowed us to access a porphyrin nanotube that contains unstable and unprecedented tetranuclear Mo^{VI}-oxo clusters in its inner space.[15] Supramolecules that are based on the self-assembly of saddle-distorted H_2DPP derivatives owing to intermolecular interactions can give isolated inner spaces for the protection of the encapsulated guest molecules from external lethal attack. This structural motif can contribute towards the stabilization unstable and metastable species in the cavity, which allows us to observe unprecedented characteristics of the molecules. Based on this strategy, we can access novel functionalities of porphyrin-based multicomponent materials at a molecular level in a well-organized manner as single crystals.

Herein, we report the formation of a novel porphyrin nanochannel (PNC; Scheme 1) that consists of porphyrin dications as electron acceptors and hydroquinone derivatives as electron donors, which are contained in the crystals, to construct unique donor–acceptor organic materials.[16] These materials are formed by molecular recognition, which depends on the electronic characteristics and the steric requirements of the guest molecules. We have also revealed that the PNC that contains electron-donating guest molecules undergoes a PET from the guest molecules to give the CS states, which results in the formation of cation radicals of the corresponding guest molecules.

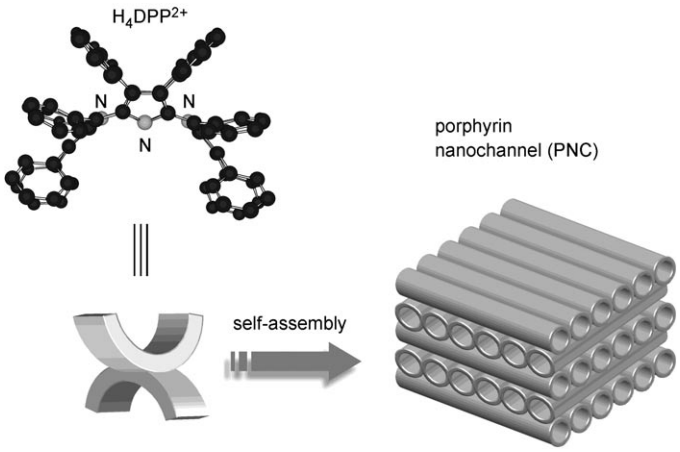

Scheme 1. Schematic representation for the formation of the PNCs.

Results and Discussion

Preparation of the PNC without guest molecules: H_2DPP was synthesized by a literature procedure[17] The chloride salt of doubly protonated H_4DPP^{2+} was obtained by adding 37% aqueous hydrochloric acid to a solution of H_2DPP in $CHCl_3$. Recrystallization of the crude product from $CHCl_3$ by vapor diffusion of CH_3CN gave crystals of a PNC that contains molecules of water and $CHCl_3$, which can be formulated as $[H_4DPP]Cl_2{\cdot}0.5(H_2O)_4{\cdot}0.5(CHCl_3){\cdot}(CH_3CN)_2$. This formulation was confirmed by both elemental analysis and integration of the signals in the ^{1}H NMR spectrum recorded in CD_2Cl_2. This compound acts as a starting material to form a variety of PNC compounds that are reported in this paper.

The crystal structure of the PNC that contains water molecules (PNC–water), $[H_4DPP]Cl_2{\cdot}0.5(H_2O)_4{\cdot}0.5(CHCl_3){\cdot}(CH_3CN)_2$, was determined by X-ray crystallography. The structure of $[H_4DPP]Cl_2$ and a packing view of the motif that contains water are shown in Figure 1. The structure of the motif that contains chloroform is given in the Supporting Information. The nanochannel structure arose from the self-assembly of $[H_4DPP]Cl_2$ as a building block and crystallized in the monoclinic $C2/c$ space group with the center of symmetry at the midpoint of the two of water molecules. Two channels run into the [1 1 0] and [1 −1 0] directions in the crystal with an angle of about 70° between them. The porphyrin dication units underwent intermolecular π–π interactions (3.44–3.59 Å) among the peripheral phenyl groups in the direction of the crystallographic c axis. The $[H_4DPP]^{2+}$ ion exhibited a larger saddle distortion compared with that of $[Mo(DPP)(O)(H_2O)]^+$ in the porphyrin

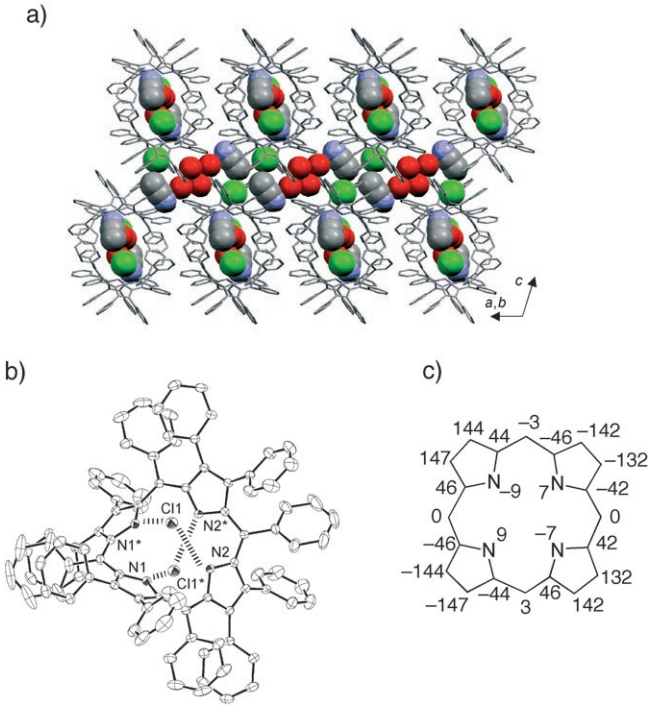

Figure 1. a) The crystal packing structure of PNC–water (carbon: gray, nitrogen: blue, oxygen: red, chloride: light green). b) An ORTEP drawing of the $[H_4DPP]Cl_2$ moiety (50% probability thermal ellipsoids) and hydrogen bonds (dotted lines). c) The displacement of each atom from the mean porphyrin plane (in units of 0.01 Å).

nanotube and the size of the channel was estimated to be 1.0×0.7 nm, which was smaller than that (1.0×1.4 nm) of the porphyrin nanotube. The chloride anions are hydrogen bonded to the N–H protons that are oriented on the upper and lower sides of the mean porphyrin plane, as shown in Figure 1b. The N–H···Cl^- distances were determined to be 3.19 to 3.23 Å. Although H_2DPP is known to exhibit some conformational flexibility,[18] these hydrogen bonds fix the conformation of the porphyrin ring so that it retains the large saddle distortion. The saddle distortion observed for $[H_4DPP]^{2+}$ can be shown by displacements of 24 atoms from the least-square mean plane, as presented in Figure 1c.

In the PNC, acetonitrile molecules are held in the cavity by π–π interactions with the *o*-position of two *meso*-phenyl groups at a distance of 3.60 Å. Four water molecules were trapped in the channel without interacting with any part of the porphyrin salt and two of them formed intermolecular hydrogen bonds to become a pair. The formation of such a PNC–water complex indicates that the supramolecular structure is the global minimum of the enthalpy driven self-assembly of $[H_4DPP]Cl_2$. The requirement for its formation is the existence of two acetonitrile molecules at the positions shown in Figure 1a. Thus, the $\{[H_4DPP]Cl_2\cdot(CH_3CN)_2\}$ moiety is recognized as a skeleton unit of PNC because other PNCs that contain various guest molecules consist of the same structural essence concomitant with guest inclusion as $[H_4DPP]Cl_2\cdot(guest)\cdot(CH_3CN)_2$, as described below. Based on the crystal structure of PNC–water, guest molecules are encapsulated in a certain position in the cavity that is composed of the skeleton unit and the position can be identified as a guest-inclusion site. The size of the guest-inclusion site was estimated to have a volume of around $10\times9\times5$ Å^3, which suggests that planar, less bulky molecules are favored.

Thermal gravimetric (TG) analysis and differential thermal analysis (DTA) of PNC–water showed a peak in the range from 386 to 437 K owing to an endothermic process, as depicted in Figure 2. Weight loss during this process was

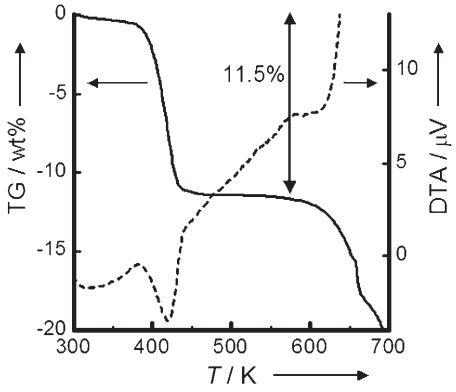

Figure 2. TG analysis (——) and DTA (-----) for PNC–water.

attributed to the elimination of all the encapsulated guest molecules, that is, CH_3CN, H_2O, and $CHCl_3$. The weight loss was 11.5% and this value was consistent with the sum of 0.5 mol of $(H_2O)_4$, 0.5 mol of $CHCl_3$, and 2 mol of CH_3CN from 1 mol of $[H_4DPP]Cl_2\cdot0.5(H_2O)_4\cdot0.5(CHCl_3)\cdot(CH_3CN)_2$, for which the calculated value was 12.1%. This result confirmed the formula of PNC–water, in addition to that of elemental analysis. At temperatures above 583 K, an exothermic peak was observed and was attributed to the thermal decomposition of $[H_4DPP]Cl_2$. This observation suggests that the nanochannel structure should be stable up to $\approx$373 K.

Absorption spectra of H_2DPP and $[H_4DPP]Cl_2$ were measured in CH_2Cl_2. Diffuse reflection spectra were also measured and converted by using a Kubelka–Munk function (Figure 3). Absorption maxima of Soret bands in solution were observed at 468 and 488 nm for H_2DPP and $[H_4DPP]Cl_2$, respectively. The redshift in the protonated form is typical for porphyrins.[19] In the solid states, those peaks were observed at 462 and 496 nm for H_2DPP and $[H_4DPP]Cl_2$, respectively. The redshift of the Soret band in the solid state relative to that in CH_2Cl_2 for the $[H_4DPP]Cl_2$ is reminiscent of such shifts observed in J aggregation of porphyrins in solution.[20] Actually, the PNC compounds exhibit π–π interactions among peripheral phenyl groups and this may cause the bathochromic shift of the Soret band.

The Q bands of H_2DPP in CH_2Cl_2 were observed at 566, 618, and 724 nm, whereas those of $[H_4DPP]Cl_2$ were observed at 650 (shoulder) and 712 nm.

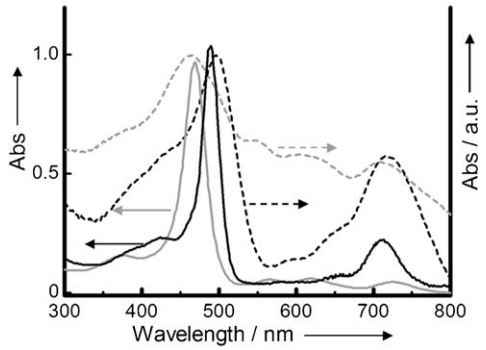

Figure 3. Absorption spectra of solutions of H_2DPP (grey ——) and $[H_4DPP]Cl_2$ (black ——) in CH_2Cl_2 and diffuse reflection of H_2DPP (grey -----) and $[H_4DPP]Cl_2$ (black -----).

Formation of PNCs that contain guest molecules: Vapor diffusion of CH_3CN into solutions of PNC–water and of guest molecules (20 equiv) in $CHCl_3$ and CH_3CN gave PNCs with the formula $[H_4DPP]Cl_2{\cdot}(guest){\cdot}(CH_3CN)_2$ in good yields, as described in the following sections. The crystals obtained were all in the monoclinic *C*2/*c* space group with the center of symmetry at the middle of the guest molecules. Previously, we reported that two molecules of acetonitrile were included as the guest,[16] however, it was found that water and chloroform molecules were in fact the guest molecules.

PNCs with hydroquinone derivatives: In the presence of hydroquinone derivatives (*o*-, *m*-, and *p*-dihydroxybenzene), tetrafluorohydroquinone, tetrachlorohydroquinone), the starting PNC (PNC–water) underwent guest exchange over the course of recrystallization in which the water molecules were replaced with a series of guest molecules. The compounds that include these guest molecules were denoted $[H_4DPP]Cl_2{\cdot}(guest){\cdot}(CH_3CN)_2$.

The crystal structure of the PNC that contains *p*-hydroquinone (PNC–H_2Q) was determined and is shown in Figure 4a. The structure of the skeleton unit is the same as that of PNC–water in which the water molecules have been replaced by hydroquinone. The hydroquinone molecule was encapsulated as a result of intermolecular π–π interactions with H_4DPP^{2+} (Figure 5a). Hydrogen bonding between the hydroxyl groups of hydroquinone with the nitrogen atoms of the acetonitrile molecules was observed in the skeleton units at a distance of 2.85 Å. This hydrogen bonding fixes the configuration of the two hydrogen atoms of the hydroxyl groups in the *trans* orientation and this stereochemistry is important to determine the electronic structure of the corresponding cation radical derived from PET.

Tetrafluorohydroquinone (H_2QF_4) was also used as a guest and added to a solution of $[H_4DPP]Cl_2$ in $CHCl_3$/CH_3CN. Vapor diffusion of CH_3CN into the solution allowed us to obtain crystals of PNC that contain H_2QF_4 in good yield. The crystal structure of PNC–H_2QF_4 is depicted in Figure 4b. The H_2QF_4 molecules are held in the cavity formed by two β-phenyl groups of adjacent pyrroles at a distance of 3.52 Å as a result of intermolecular π–π interactions. In addition, the hydroxyl group of H_2QF_4 is directed

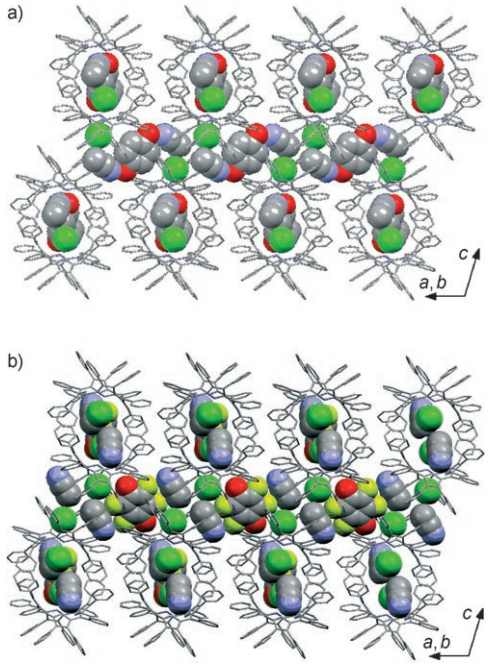

Figure 4. Crystal structures of PNC–H_2Q (a) and PNC–H_2QF_4 (b). The H_4DPP^{2+} unit is described with a wire frame. Carbon: gray, oxygen: red, nitrogen: blue, fluorine: yellow, chloride: light green.

towards the two pyrrole nitrogen atoms to exert an OH–π interaction to connect the C2–N1–C5 (C_α–N–C_α) region of the pyrroles at distances of 2.69 to 3.15 Å. These OH–π interactions are not found in PNC–H_2Q, probably because of the stronger acidity of H_2QF_4 compared with that of H_2Q, which results in a change in the direction of the OH groups in the nanochannel (see Figure 5b). These OH–π interactions also fix the orientation of the hydroxyl groups in the *trans* orientation. Thus, the orientation of the guest molecules can be regulated by their electronic characteristics.

Confirmation of the inclusion of the guest molecules obtained from the results of NMR spectroscopy for solutions of the PNC compounds. For PNC–H_2QF_4, a ^{19}F NMR spectrum was recorded of a solution in $CDCl_3$. Two singlets at $\delta = -165.37$ and -165.35 ppm were observed and these chemical shifts were in agreement with those of an authentic sample of H_2QF_4.

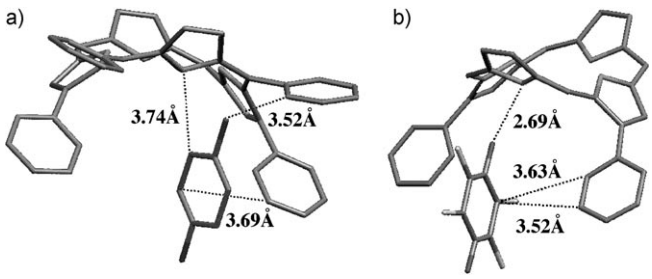

Figure 5. The difference of orientation and interactions of the guest molecules and noncovalent interactions (dotted lines) for a) H_2Q and b) H_2QF_4.

We also confirmed the inclusion of tetrachlorohydroquinone (H_2QCl_4) in the PNC based on elemental analysis results, although X-ray crystallographic analysis was unsuccessful for this material. In sharp contrast, tetrabromohydroquinone was not encapsulated in the PNC, probably owing to the larger atomic radius of bromine, which results in steric hindrance in the guest-inclusion site.

Driving force of guest encapsulation: During guest encapsulation, the guest molecules should interact with $[H_4DPP]Cl_2$ in solution. We have previously proposed that the inclusion of hydroquinone is induced by hydrogen bonding of the hydroxyl groups with the Cl^- ion of $[H_4DPP]Cl_2$, based on the results of variable-temperature ^1H NMR measurements.[16] However, no inclusion of 1,4-dihydroxy-*p*-benzoquinone, which also has two hydroxyl groups, in the PNC was observed and instead PNC–water was formed. Therefore, we realized that hydrogen bonding of guest molecules with $[H_4DPP]Cl_2$ in solution was not a determining factor for the formation of a guest-encapsulated PNC architecture.

In the case of benzoquinone derivatives, which are two-electron oxidized species of the corresponding hydroquinones, no encapsulation was observed for these molecules under the same conditions. The lack of encapsulation was confirmed by X-ray crystallography, elemental analysis, and ^1H and ^{19}F NMR spectroscopy for the crystals formed by the recrystallization of $[H_4DPP]Cl_2$ with quinones (benzoquinone, tetrafluorobenzoquinone, and tetrachlorobenzoquinone). These results indicate that electron-donating molecules are encapsulated selectively. Thus, PNC recognizes the electronic character of guest molecules, rather than specific functional groups or shapes in the molecules. This selection rule stems from the cationic character of H_4DPP^{2+} that favors electron-rich substrates owing to electrostatic donor–acceptor interactions, as observed in organic conductors and semiconductors.[21,22]

When tetrabromohydroquinone (H_2QBr_4) was employed as a guest molecule, however, H_2QBr_4 was not encapsulated in the PNC. This indicates that steric factors are also important for PNC–guest formation. To assess the steric effects of guest molecules in encapsulation phenomena, we used xylene isomers as guest molecules. As reference experiments, we confirmed that all of the xylene isomers could be encapsulated into the PNCs based on elemental analysis and ^1H NMR spectroscopy for the crystalline samples obtained by the recrystallization of $[H_4DPP]Cl_2$ in the presence of a large excess of each isomer. X-ray crystallography on a single crystal obtained by using *p*-xylene as the guest molecule revealed that *p*-xylene molecules were contained within the PNCs to form PNC–*p*-xylene, and its crystal structure is shown in Figure S1a in the Supporting Information. The skeleton unit is the same as the other PNC compounds described above. One β-phenyl group of $[H_4DPP]^{2+}$ was found to have weak π–π interactions with the xylene guest molecule at a distance of 3.64 to 3.69 Å (Figure S1b in the Supporting Information).

To estimate the steric influence on guest encapulation, we used an equimolar mixture of *o*-, *m*-, and *p*-xylene as the guest molecules. Recrystallization of $[H_4DPP]Cl_2$ from $CHCl_3/CH_3CN$ in the presence of a large excess of the mixture gave crystals of PNC that contained xylene molecules. The crystalline material was dissolved in $CDCl_3$ to measure its ^1H NMR spectrum. The spectrum showed peaks that were assigned to each isomer of xylenes. Deconvolution of overlapping peaks was performed by using a 1D NMR program[23]. Curve fitting allowed us to determine the ratio of encapsulated xylene isomers to be 1:1:5 for *o*/*m*/*p*. This result indicates that the shape of the guest-inclusion site exerts steric effects to select the guest molecule, which supports our proposal that the lack of encapsulation of H_2QBr_4 results from its larger size compared with that of the encapsulated hydroquinone derivatives. The ratio observed in the competitive encapsulation of xylene isomers should be determined kinetically rather than thermodynamically because all of the isomers could be included intrinsically within the guest-inclusion site, as described above. Thus, the PNC superstructure exhibits selective encapsulation primarily based on the electronic characteristics and secondly based on the shape and size of the guest molecules. Our results indicate that guest inclusion into the PNC is not mere clathrate formation as reported by Strouse and co-workers[24] and Goldberg.[25]

PET from hydroquinones to $[H_4DPP]Cl_2$: As the principal factor for guest encapsulation, the guest molecules are required to have electron-donating characteristics. Generally, neutral porphyrin compounds, which includes free bases and metal complexes, have been recognized as electron donors in PET.[26] In contrast, cationic porphyrin complexes have been reported to act as electron acceptors.[27] The H_4DPP^{2+} moiety in the PNC is positively charged, and therefore, hard to oxidize. Hence, it is reasonable to expect that PET can occur from the guest donor molecules to the electron acceptor, $[H_4DPP]Cl_2$, in the skeleton unit. To prove this expectation, we measured ESR spectra of PNC–guest crystals under photoirradiation ($\lambda > 340$ nm) at room temperature.[28] The infrared region was cut off by using a water filter to avoid both thermal excitation and decomposition of the compounds. The observed ESR spectra are shown in Figure 6 together with spectra obtained from computer simulations and the hyperfine coupling constants (hfc) used are also given. The hfc values of hydroquinone cation radicals were calculated by using density functional theory (DFT) calculations at the UB3LYP/6-31G* level. The assignment of the hfc values for the hydroquinone cation radicals in Figure 6 was made based on the comparison between the calculated and observed values (see below).

It should be noted that the configuration of both OH groups of H_2Q are fixed in the *trans* orientation in the PNC guest-inclusion site as a result of hydrogen bonding with the acetonitrile molecules (see above). It has been reported that $H_2Q^{+\bullet}$ undergoes *cis–trans* isomerization in solution to give ESR spectra for a mixture of isomers at $< -20\,^\circ C$ in

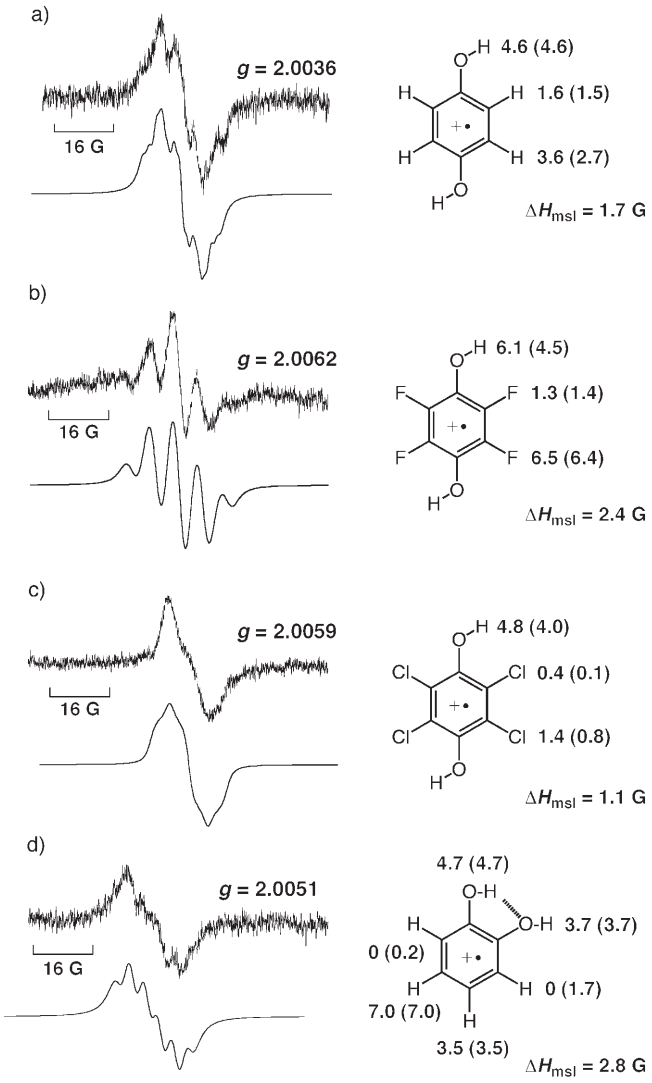

Figure 6. ESR spectra of cation radicals of the guest molecules in a) PNC–H_2Q, b) PNC–H_2QF_4, c) PNC–H_2QCl_4, and d) PNC–Cat in the crystals at room temperature under photoirradiation ($\lambda > 340$ nm). The upper traces are the observed spectra and the lower traces are their computer simulations. The hfc values (in gauss) used for the simulations are indicated on the structures of the cation radicals and those values obtained from DFT calculations are given in parentheses. ΔH_{msl} represents the maximum slope line width used for simulations.

CH_3NO_2.[29] In addition, the cation radicals of hydroquinone and catechol are known to be strong acids with pK_a values of -0.8 and -1.65, respectively.[30] In the case of PNC–H_2Q (Figure 6a), there are three sets of hfc values as a result of two equivalents protons (4.6, 3.6, and 1.6 G). These hfc values are more in agreement with those calculated for the *trans* isomer of $H_2Q^{+\bullet}$ (4.6, 2.7 and 1.5 G) rather than those for the *cis* isomer (4.6, 2.4, and 1.8 G).[31] The largest hfc value (4.6 G) is assigned to the OH proton and the difference between two CH protons for the *trans* isomer is significantly larger than that for the *cis* isomer. In the case of PNC–H_2QF_4, the difference between the two a_F (hfc of the F nuclei) values of $H_2QF_4^{+\bullet}$ becomes more pronounced for the *trans* isomer (Figure 6b). A similar trend is also observed for PNC–H_2QCl_4 in Figure 6c, in which there is large difference between the two a_{Cl} (hfc of the Cl nuclei) values of $H_2QCl_4^{+\bullet}$, although the large line width does not allow the accurate determination of the smaller a_{Cl} value. Thus, the ESR signals due to $H_2Q^{+\bullet}$ and its derivatives indicate that the configuration of the cation radicals is fixed in the *trans* geometry as in the neutral form in the PNC crystal structure. In the case of PNC–Cat (Cat = catechol (*o*-hydroquinone)), the ESR signal in Figure 6d is assigned to the catechol cation radical based on a comparison between the observed and calculated hfc values. The hydroquinone and catechol cation radicals survive for around two hours at room temperature without deprotonation after light has been blocked from the sample. The observation of the cation radicals of guest molecules shown in Figure 6 clearly indicates the occurrence of PET from guest molecules to H_4DPP^{2+} in the PNC–guest crystals. The absence of $H_4DPP^{+\bullet}$, which should also be produced together with cation radicals of guest molecules during PET, is discussed in the following sections.

Energetics of PET: To determine the energetics of PET in the PNC–guest crystals, the redox potentials and excitation energies of H_4DPP^{2+} and the guest molecules were determined by electrochemical and photophysical measurements. The cyclic voltammogram (CV) of $[H_4DPP]Cl_2$ in CH_2Cl_2 that contained 0.1 M tetrabutylammonium perchlorate (TBAP) as an electrolyte exhibits a quasi-reversible reduction wave at -0.46 V (vs. SCE), which was assigned to the two-electron redox couple of H_4DPP^{2+}/H_4DPP (see Figure S5 in the Supporting Information) because the disproportionation of one-electron reduced species of protonated porphyrins is known to occur rapidly.[32] The redox titration of $[H_4DPP]Cl_2$ with bis(cyclopentadienyl)cobalt(II) ($CoCp_2$) in $CHCl_3$ allowed us to confirm that the redox process is a two-electron process (Figure 7) in which two equivalents of $CoCp_2$ is consumed in the reduction of H_4DPP^{2+}. The CVs of the catechol and hydroquinone derivatives exhibits an irreversible oxidation wave because of the facile deprotona-

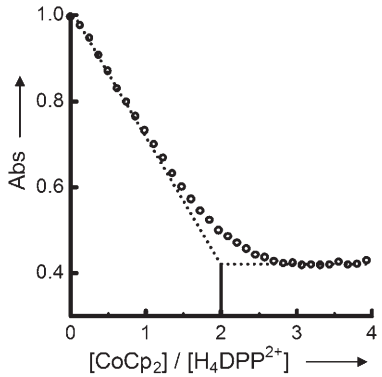

Figure 7. Redox titration of $[H_4DPP]Cl_2$ with $CoCp_2$ in $CHCl_3$ at room temperature. The absorbance at 489 nm was followed over the course of the titration.

tion of the cation radicals. The oxidation potentials of the catechol and hydroquinone derivatives (E_{ox}) were determined by using second harmonic ac voltammetry (SHACV) and the E_{ox} values obtained are listed in Table 1 in which the HOMO energies were calculated by DFT methods at the B3LYP/6-31G* level.[33]

Table 1. Oxidation potentials of guest molecules and rate constants of charge separation (k_{CS}), disproportionation (k_{DIS}) and charge recombination (k_{CR}) for PNC–guest.

	HOMO [eV][a]	E_{ox} (V vs. SCE)[b]	k_{CS} [s^{-1}]	$k_{DIS}+k_{CR}$ [s^{-1}]
$[H_4DPP]Cl_2$		1.26[c]		
PNC–H_2Q	−5.41	1.09	$(2.1\pm0.2)\times10^{11}$	$(2.2\pm0.3)\times10^{10}$
PNC–Cat	−5.62	1.20	$(1.6\pm0.2)\times10^{11}$	$(1.8\pm0.2)\times10^{10}$
PNC–H_2QF_4	−6.19	1.37	$(1.3\pm0.1)\times10^{11}$	$(9.4\pm1.2)\times10^{9}$
PNC–H_2QCl_4	−6.31	1.39	$(1.0\pm0.1)\times10^{11}$	$(9.4\pm1.2)\times10^{9}$

[a] Calculated at the B3LYP/6-31G* level of theory. [b] Determined by SHACV performed in dichloromethane at room temperature under N_2 in the presence of TBAP (0.1 M). [c] Oxidation potential of $^1(H_4DPP^{2+})^*$, which was estimated to be 1.72−0.46 = 1.26 V.

The singlet excited-state energy (S_1) of $[H_4DPP]Cl_2$ was determined from the fluorescence maximum (731 nm) and the absorption maximum (712 nm) in argon-bubbled CH_2Cl_2 was 1.72 eV (Figure S2 in the Supporting Information).[34] The triplet excited-state energy (T_1) was determined from the phosphorescence (838 nm) at 77 K as 1.48 eV (Figure S3 in the Supporting Information). From the E_{ox} values of the guest molecules and the E_{red} value of H_4DPP^{2+}, the energies of the charge-separated states were determined to be those shown in Figure 8. The PET from *p*-H_2Q and *o*-H_2Q to $^1(H_4DPP^{2+})^*$ is thermodynamically feasible, whereas the PET from H_2QF_4 and H_2QCl_4 to $^1(H_4DPP^{2+})^*$ is slightly endergonic in CH_2Cl_2. The occurrence of PET from H_2QF_4 and H_2QCl_4 to $^1(H_4DPP^{2+})^*$ to produce the cation radicals of guest molecules in Figure 6b and c indicates that the E_{ox} values of hydroquinones in the PNC–guest crystals may be shifted in the negative direction owing to hydrogen bonding with the nitrogen atoms of the acetonitrile molecules in the skeleton units (see above). In all instances PET from the guest molecules to the triplet excited state ($^3(H_4DPP^{2+})^*$) is energetically unlikely to occur.

Laser flash photolysis: To gain mechanistic insights into PET in the PNC, femtosecond laser flash photolysis was performed in the solid state on PNC samples as KBr pellets.[35] As a reference test, a KBr pellet that did not contain a PNC sample did not show any absorption over the course of laser flash photolysis at 355 nm. In contrast, the transient absorption spectra of PNC–H_2Q are shown in Figure 9a. The transient absorption spectrum observed at 1.5 ps, which has an absorption maximum at 580 nm and bleaching at 500 nm is assigned to the singlet excited state, $^1(H_4DPP^{2+})^*$.[36] The decay of absorption at 620 nm owing to $^1(H_4DPP^{2+})^*$ is accompanied by a rise in the absorption at 530 nm (Figure 9b). The transient absorption spectrum at 25 ps may be assigned to $H_4DPP^{+\bullet}$ produced by PET from H_2Q to $^1(H_4DPP^{2+})^*$ (see below). The PET rate constant was determined to be $2.1\times10^{11}\ s^{-1}$ at 298 K. At 2000 ps (2 ns), the transient absorption spectrum again changes to that owing to the triplet excited state of the dication, $^3(H_4DPP^{2+})^*$. The absorption derived from $H_2Q^{+\bullet}$ was reported to have an absorption maximum at 423 nm.[37] Thus, this absorption does not perturb the absorption spectra of the porphyrin-derived species described above.

Assignments of the transient absorptions in Figure 9 were made by nanosecond laser flash photolysis at 430 nm on $[H_4DPP]Cl_2$ (1.0×10^{-5} M) and are shown in Figure 10. In deaerated benzonitrile, we observed a transient absorption attributed to the triplet excited state of $[H_4DPP]Cl_2$ ($^3(H_4DPP^{2+})^*$) with the absorption maximum at 560 nm (Figure 10a). In the presence of an excess of ferrocene (15 mM), PET from ferrocene to $^3(H_4DPP^{2+})^*$ occurs to afford $H_4DPP^{+\bullet}$, which exhibits the absorption maximum at 530 nm (Figure 10b). In the absence of ferrocene, $^3(H_4DPP^{2+})^*$ decays slowly over a ten microsecond timescale, whereas the decay is significantly enhanced owing to PET from ferrocene to $^3(H_4DPP^{2+})^*$, as shown in Figure 10c. The PET rate constant was determined to be $2.5\times10^{8}\ M^{-1}\ s^{-1}$.

A comparison of the transient absorption spectrum observed at 25 ps after laser excitation at 355 nm in Figure 9a with that in Figure 10b confirms that $H_4DPP^{+\bullet}$ is produced by PET from H_2Q to $^1(H_4DPP^{2+})^*$.

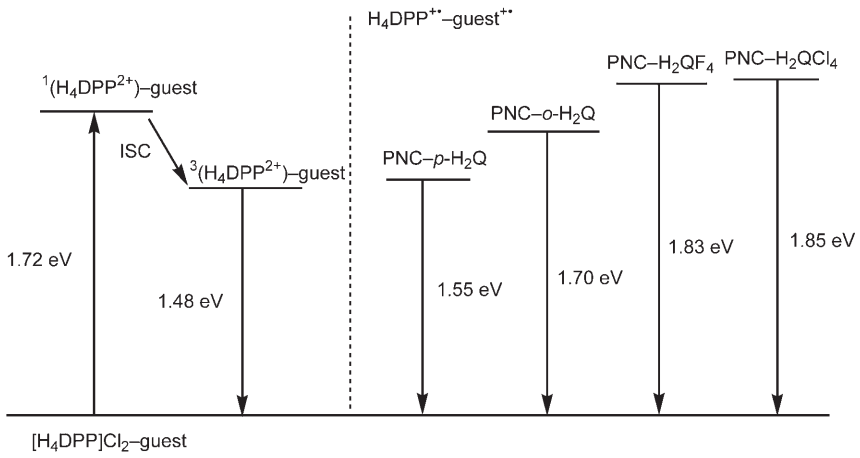

Figure 8. Energy diagrams for photoexcitation of PNC and the charge-separation states of the PNC–guest molecules.

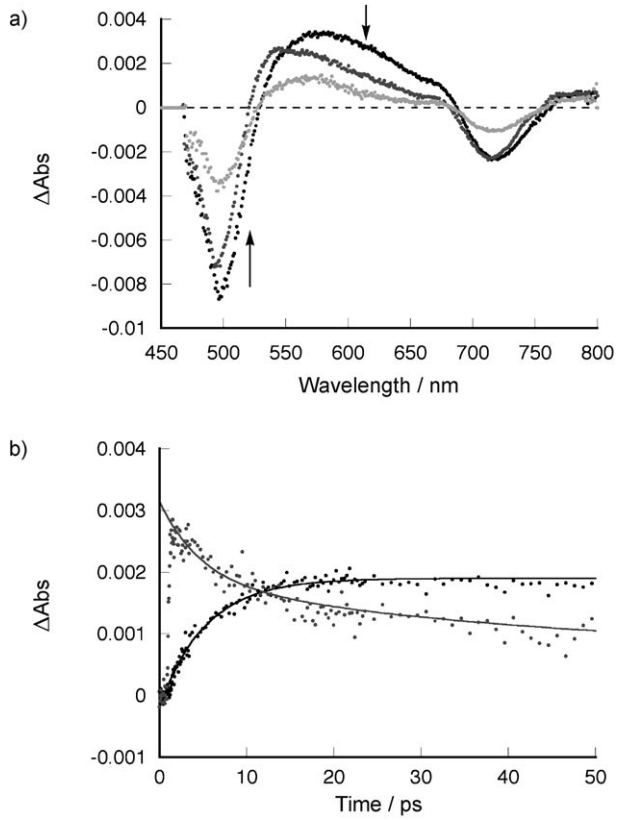

Figure 9. Femtosecond laser flash photolysis of PNC–H_2Q with excitation at 355 nm of a KBr pellet containing the PNC sample: a) transient absorption spectra at 1.5 ps (black), 25 ps (dark grey), and 2000 ps (pale grey) and b) decay and rise of the absorption at 620 nm (grey) and 530 nm (black).

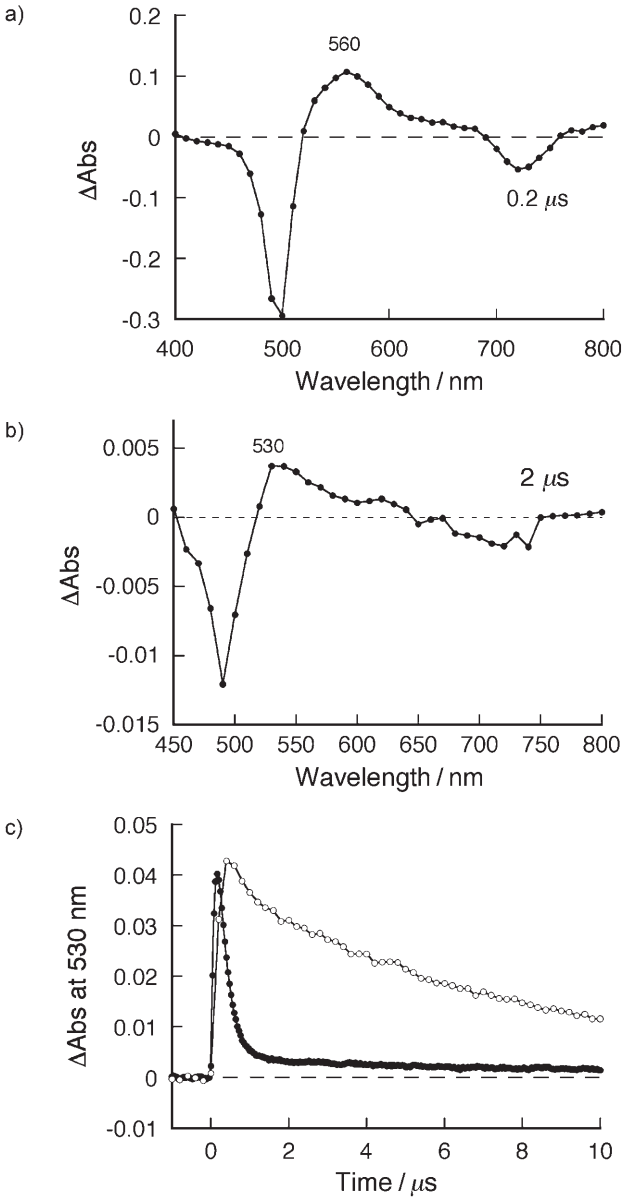

Figure 10. Transient absorption spectra of a) $^3(H_4DPP^{2+})^*$ ($[H_4DPPCl_2]=1.0\times10^{-5}$ M in deaerated PhCN) and b) $H_4DPP^{+\bullet}$ ($[H_4DPPCl_2]=1.0\times10^{-5}$ M and [Ferrocene] = 15 mM in deaerated PhCN). Excitation at 430 nm by using an Nd/YAG laser. c) Rise and decay of the absorption at 530 nm in the absence (○) or presence (●) of ferrocene (15 mM).

The decay in the absorbance at 530 nm owing to $H_4DPP^{+\bullet}$ on the 0 to 2000 ps timescale indicates that $H_4DPP^{+\bullet}$ decays by undergoing bimolecular reactions (see the linear second-order plot in the inset of Figure 11). The bimolecular decay involves disproportionation of $H_4DPP^{+\bullet}$ and back electron transfer from $H_4DPP^{+\bullet}$ to $H_2Q^{+\bullet}$ to produce the triplet excited state, $^3(H_4DPP^{2+})^*$ because the triplet excited energy of H_4DPP^{2+} is lower than the charge-separated state (see Figure 8). The disproportionation of $H_4DPP^{+\bullet}$ may proceed rapidly through electron hopping between $H_4DPP^{+\bullet}$ and H_4DPP^{2+} in the PNC–H_2Q crystals, which results in the formation of $H_2Q^{+\bullet}$ that remains the stable product (Figure 6).

The charge separation rate constants (k_{CS}) for other PNC–guest systems have also been determined by femtosecond laser flash photolysis and the results are summarized in Table 1. Table 1 shows that the k_{CS} value increases as the oxidation potentials and HOMO energies of the guest molecules decrease, that is, the easier it is to oxidize the sample then the faster the charge separation occurs. The decay rate constants of $H_4DPP^{+\bullet}$ in these systems, which correspond to the disproportionation (k_{DIS}) and the charge recombination (k_{CR}), were also determined and are listed in Table 1. In addition to evidence from the transient absorption spectrum, we also confirmed the formation of $^3(H_4DPP^{2+})^*$ by time-resolved electron spin resonance (TRESR) spectroscopy with excitation at 585 nm. The simulation allowed us to estimate the zero-field splitting parameters as $D=(-3/2)E_z=0.93$ GHz and $2E=E_x-E_y=0.0$ GHz, which are typical values for the excited triplet states of porphyrins.[38,39] The population ratio of the sublevel for $P_x/P_y/P_z$ was 0.0:0.2:0.8. The deviation of the signal from the simulation may result from fast excitation hopping over the porphyrin arrays in the PNC crystals. The absence of a TRESR signal from $H_2Q^{+\bullet}$ indicates that the singlet radicals cannot be polarized in the solid state in which separation and re-encounter of the radicals, which is required for the radical pair mecha-

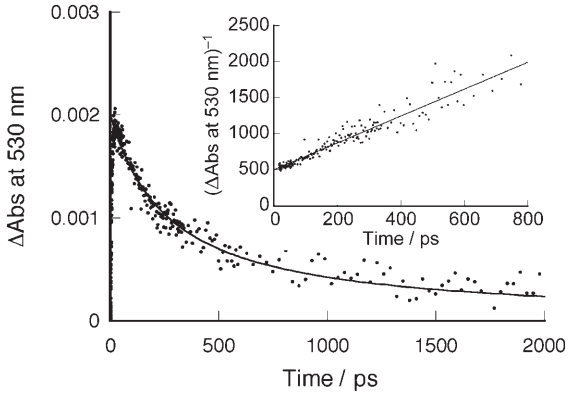

Figure 11. Decay profile of the absorption at 530 nm owing to $H_4DPP^{+\bullet}$ produced upon photoexcitation of PNC–H_2Q at 355 nm in a KBr pellet. The inset shows the second order plot.

nism,[40] is unlikely to occur. The recombination of the geminate radical ions yields the observed triplet signal shown in Figure 12. The observation of the stable $H_2Q^{+\bullet}$ in the cw

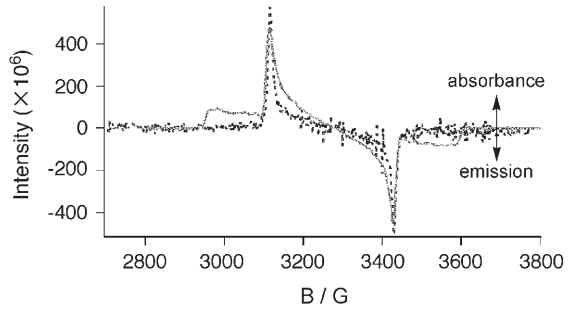

Figure 12. TRESR spectrum of PNC–H_2Q as a powder. Experimental data (-----) and its simulation (——) are overlaid. Conditions: magnetic field = 2708–3778 G, ν = 9.14976 GHz, λ = 585 nm, OPO laser, microwave = 1 mW, room temperature, time delay = 1 μs.

ESR experiments results from the disappearance of $H_4DPP^{+\bullet}$ that is produced together with $H_2Q^{+\bullet}$ through the disproportionation of $H_4DPP^{+\bullet}$ (see above).

We can summarize the photodynamics, as shown in Scheme 2, by using PNC–H_2Q as a representative compound. The photoirradiation of PNC–H_2Q affords the singlet excited state of the porphyrin dication, $^1(H_4DPP^{2+})^*$, which can be observed by femtosecond laser flash photolysis. The excited singlet state of the porphyrin accepts one electron from the H_2Q guest molecule to give the corresponding radical cation by PET. The oxidation potentials of H_2Q and Cat are 1.09 and 1.20 V, respectively, and these values are lower than that of $^1(H_4DPP^{2+})^*$ (1.26 V) to allow the PET process to become energetically feasible. The reduced cation radical, $H_4DPP^{+\bullet}$, undergoes

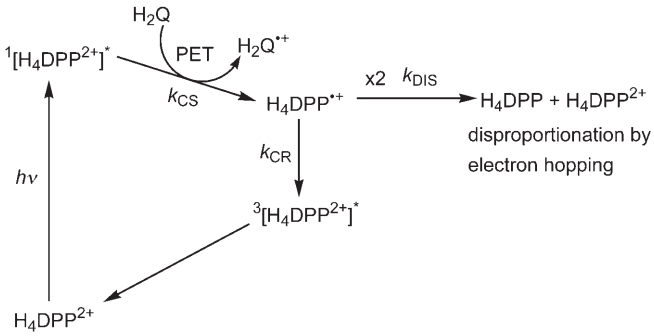

Scheme 2. Summary of photochemical events in PNC–H_2Q as a representative.

fast disproportionation based on electron hopping in the solid state owing to close contacts with other H_4DPP^{2+} molecules through intermolecular π–π interactions to give the original H_4DPP^{2+} species and the two-electron reduced species of H_4DPP. In addition, $H_4DPP^{+\bullet}$ undergoes back electron transfer (charge recombination) to form $^3(H_4DPP^{2+})^*$, the energy of which is lower than that of the charge-separated state described in Figure 8.

The guest molecules form intermolecular hydrogen bonds with acetonitrile for H_2Q as the guest molecule and the pyrrole nitrogen atoms for H_2QF_4 (Figure 13). The pyrrole nitrogen is protonated, however, the interaction of the chloride anion with the pyrrole nitrogen atom through hydrogen bonding should reduce the positive charge on the nitrogen to accommodate the intermolecular hydrogen bonds with H_2QF_4 by the π electrons of pyrrole. This hydrogen bonding may lower the oxidation potential of H_2QF_4, which would otherwise be impossible to be oxidized by the S_1 state of $[H_4DPP]Cl_2$ (1.72 eV). We can assume that similar intermolecular hydrogen bonds operate to reduce the oxidation potential of H_2QCl_4 that is oxidized to form the corresponding radical cation. These arguments are strongly supported by lowering the oxidation potentials by intramolecular hydrogen bonding in bis-phenol derivatives.[41]

Conclusion

The self-assembly of the saddle-distorted $[H_4DPP]Cl_2$ unit gives a channel structure that is composed of channels of

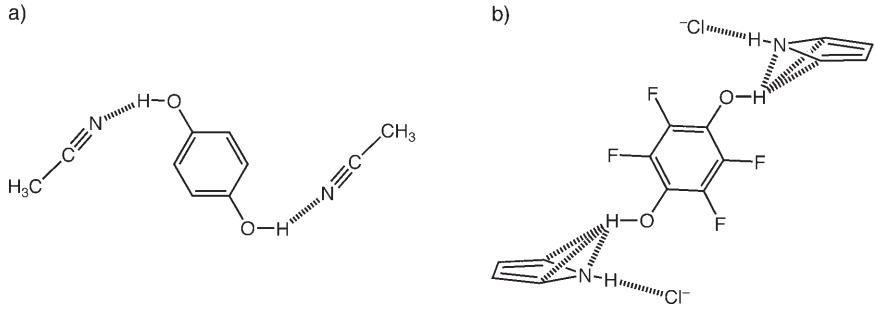

Figure 13. Schematic description of specific intermolecular hydrogen bonding for a) PNC–H_2Q and b) OH–π interactions in PNC–H_2QF_4.

around one nanometer in diameter. The channels are formed as the thermodynamic global minimum and are able to include guest molecules depending on their electronic characteristics and steric effects. The selectivity of guest encapsulation in the channel is dependent upon the electronic characteristics of the guest molecules, electron-donating guests are vital, whereas electron acceptors are not encapsulated in the PNC. This feature of guest recognition, based on the electronic characteristics of the guest, is unique and provides a new category of molecular organic functional materials.[42] Concerning the steric effects, the size of the guest molecules should fit into the guest-inclusion site, which has a volume of around $10\times9\times5$ Å^3 and suggests that planar and less bulky molecules are favored.

PNCs that contain electron-donating molecules undergo PET to allow us to observe unusually stabilized cation radicals of the guest molecules upon photoirradiation at room temperature. The electronic structures of the radicals were determined by ESR spectroscopy in combination with DFT calculations. PET proceeds via the singlet excited state of H_4DPP^{2+}, which accepts one electron from an electron donor in the encapsulation site and forms $H_4DPP^{+\bullet}$ that undergoes fast disproportionation to give diamagnetic species, such as H_4DPP^{2+} and H_4DPP. Photodynamics of this charge-separation process were revealed by solid-state femtosecond laser flash photolysis. The PET rate constant increases as the oxidation potentials and ionization energies (E_{HOMO}) of the guest molecules decrease. The PET process to $^1(H_4DPP^{2+})^*$ proceeds much more efficiently than the intersystem crossing to give the triplet excited state, $^3(H_4DPP^{2+})^*$, owing to close and secure contact and inevitable intermolecular interactions with the guest molecules in the PNC. Thus, PNCs can be used as the basis for constructing and developing porphyrin-based photofunctional materials.

Experimental Section

General: Chemicals were purchased from commercial sources and used without further purification unless otherwise noted. Toluene was distilled over sodium-benzophenone ketyl and was used for the synthesis of H_2DPP. $CHCl_3$, CH_3CN, and CH_2Cl_2 were distilled over CaH_2 before use.

Apparatus: Absorption spectra were recorded as solutions in CH_2Cl_2 by using a Jasco V-570 spectrophotometer in the range of $\lambda=200$ to 2000 nm at room temperature. Diffuse reflection spectra were measured by using the same apparatus equipped with a Jasco ISN-470 60 mmϕ integrating sphere attachment. The reflectance spectra obtained were converted to absorption spectra by using the Kubelka–Munk function $F(R_8)$. IR spectra were recorded by using a ThermoNicolet NEXUS 670 FTIR spectrometer in the range of $\tilde{\nu}=400$ to 4000 cm^{-1} at room temperature. Samples were prepared as KBr pellets at a concentration of 0.5%. ^{1}H and ^{19}F NMR spectra were measured by using JEOL AL-300 and Bruker DPX 400 spectrometers, respectively. The fluorescence spectrum was obtained with a quartz cell (1 cm) at room temperature for an argon-bubbled solution of H_4DPPCl_2 in $CHCl_3$ by excitation at 496 nm by using a Shimadzu RF-5300PC spectrofluorophotometer. The phosphorescence spectrum was recorded in a quartz tube (3 mm in diameter) in a liquid nitrogen Dewar. A deaerated 2-methyltetrahydrofuran vial that contained H_4DPP (1.0×10^{-5} M) at 77 K was excited at 490 nm by using a Cosmo System LVU-200S spectrometer. Near-IR emission spectra were measured by using a SPEX Fluorolog $\tau3$ fluorescence spectrophotometer. A photomultiplier (Hamamatsu Photonics, R5509-72) was used to detect emission in the near-IR region.

Preparation of $[H_4DPP]Cl_2$: The synthesis of H_2DPP was performed in accordance with a literature procedure.[17] Crude $[H_4DPP]Cl_2$ was prepared by adding 3% aqueous HCl (100 mL) to a solution of H_2DPP (1.0 g, 0.8 mmol) in CH_2Cl_2 (500 mL) in a separating funnel. The organic layer was dried over Na_2SO_4. The solvent was removed by using a rotary evaporator and the product was dried in vacuo at 120 °C. The reaction proceeded quantitatively.

Preparation of PNC–guest: The crystals of PNCs that contain various guest molecules, such as H_2Q, Cat, H_2QF_4, and H_2QCl_4, were obtained by the recrystallization of $[H_4DPP]Cl_2$ in the presence of the guest molecule (20 equiv) from $CHCl_3/CH_3CN$ (3:1 *v*/*v*) by vapor diffusion of CH_3CN at room temperature. In the case of xylene, an excess amount of each isomer was used as a substrate under the same conditions. The results of elemental analysis are summarized in Table S1 in the Supporting Information.

X-ray crystallography: The crystal structures of PNCs that contain water and chloroform (PNC–water), hydroquinone (PNC–H_2Q), tetrafluorohydroquinone (PNC–H_2QF_4), and *p*-xylene (PNC–*p*-xylene) guest molecules were determined by X-ray crystallography. The single crystals were mounted on glass fibers by using silicon grease. All diffraction data were collected by using a Rigaku/MSC Mercury CCD diffractometer at −170 °C by using graphite-monochromated $Mo_{K\alpha}$ ($\lambda=0.71070$ Å) by 2θ-ω scan. All calculations were performed on a PC by using the CrystalStructure program package.[43] The structures were solved by direct methods by using SIR97 and SHELX-97.[44] Crystallographic data for these compounds are summarized in Table 2. CCDC-626215 (PNC–water), -247692

Table 2. Crystallographic data for PNC–water, PNC–H_2Q, PNC–H_2QF_4, and PNC–*p*-xylene.

Compound	PNC–water[a]	PNC–H_2Q	PNC–H_2QF_4	PNC–*p*-xylene
formula	$C_{96.50}H_{70}N_6O_2Cl_{3.50}$	$C_{102}H_{68}N_6O_2Cl_2$	$C_{102}H_{72}F_4O_2Cl_2N_6$	$C_{104}H_{81}Cl_2N_6$
M_r	1469.66	1480.60	1560.63	1485.73
crystal system	monoclinic	monoclinic	monoclinic	monoclinic
space group	*C*2/*c*	*C*2/*c*	*C*2/*c*	*C*2/*c*
T [K]	−130	−140	−140	−130
a [Å]	17.3762(10)	17.510(5)	17.3626(17)	17.445(4)
b [Å]	24.7840(10)	24.761(6)	24.4826(19)	24.719(5)
c [Å]	19.5076(10)	19.857(5)	19.8048(18)	19.574(4)
β [°]	108.4274(7)	108.711(4)	107.9986(13)	108.938(3)
V [Å^3]	7970.2(7)	8043.7	8006.7(12)	7984(3)
Z	4	4	4	4
ρ_{calcd} [g cm^{-3}]	1.205	1.223	1.295	1.236
μ ($Mo_{K\alpha}$) [cm^{-1}]	1.908	1.37	1.478	1.361
reflns measured	30864		30402	30355
reflns unique	9081	9012	9154	9051
R_{int}	0.032		0.059	0.094
R[b]	0.0882		0.1028 ($I>3.00\sigma(I)$)	0.1126
Rw[c]	0.2461	0.238	0.1227 ($I>3.00\sigma(I)$)	0.2488
$R1$[c]	0.0830 ($I>2.00\sigma(I)$)	0.082 ($I>2.00\sigma(I)$)	0.1028 ($I>3.00\sigma(I)$)	0.1021 ($I>2.00\sigma(I)$)
GOF	1.101	1.325	1.440	1.459

[a] In this case, populations of two water molecules and one $CHCl_3$ molecule were fixed at 50% for the refinements. The water molecules were refined isotropically. [b] $R=\Sigma(Fo^2-Fc^2)/\Sigma Fo^2$. [b] $Rw=[\Sigma(w(Fo^2-Fc^2)^2)/\Sigma w(Fo^2)^2]^{1/2}$. [c] $R1=\Sigma||Fo|-|Fc||/\Sigma|Fo|$.

(PNC–H_2Q), -626214 (PNC–H_2QF_4), and -626216 (PNC–*p*-xylene) contain the supplementary crystallographic data for this paper. These data can be obtained free of charge from the Cambridge Crystallographic Data Centre via www.ccdc.cam.ac.uk/data_request/cif.

Electrochemical measurements: All of the measurements were carried out in CH_2Cl_2 that contained 0.1 M TBAP as an electrolyte at room temperature by using a BAS model ALS-720 instrument with platinum wire as a counter electrode, glassy carbon as a working electrode, and Ag/$AgNO_3$ as a reference electrode.

TG analysis and DTA: TG analysis and DTA measurements on PNC–water were performed by using a Brucker TG-DTA/M56510 instrument with a heating rate of 10 K min^{-1} in the range from room temperature to 773 K under a flow of dinitrogen.

Laser flash photolysis: Femtosecond laser flash photolysis was conducted by using a Clark-MXR 2010 laser system and an optical detection system provided by Ultrafast Systems (Helios). The source for the pump and probe pulses were derived from the fundamental output of a Clark laser system (775 nm, 1 mJ per pulse, and fwhm 150 fs) at a repetition rate of 1 kHz. A second harmonic generator introduced in the path of the laser beam provided 355 nm laser pulses for excitation; 95% of the fundamental output of the laser was used to generate the second harmonic, whereas 5% of the deflected output was used for white light generation. Prior to generating the probe continuum, the laser pulse was fed to a delay line that provided an experimental time window of 1.6 ns with a maximum step resolution of 7 fs. The pump beam was attenuated at 5 μJ per pulse with a spot size of 2 mm in diameter at the sample cell at which it was merged with the white probe pulse in a close angle ($<10°$). The probe beam, after passing through the 2 mm sample cell, was focused on a 200 μm fiber optic cable that was connected to a CCD spectrograph (Ocean Optics, S2000-UV-vis) for recording the time-resolved spectra (425–800 nm). Typically, 5000 excitation pulses were averaged to obtain the transient spectrum at a set delay time. The kinetic traces at appropriate wavelengths were assembled from the time-resolved spectral data. All measurements were performed by using potassium bromide pellets that contained PNC at 298 K.

Measurements of transient absorption spectra of the H_4DPP radical cation were performed according to the following procedure: A deaerated solution that contained H_4DPP (1.0×10^{-5} M) and ferrocene (4.0×10^{-2} M) in PhCN was excited by Nd/YAG laser (Continuum, SLII-10, fwhm 4–6 ns) at 430 nm. Time courses of the transient absorption spectra were measured by using a continuous Xe lamp (150 W) and an In GaAs PIN photodiode (Hamamatsu 2949) as a probe light and a detector, respectively. The output from the photodiodes and a photomultiplier tube was recorded by using a digitizing oscilloscope (Tektronix, TDS3032, 300 MHz). The transient spectra were measured by using fresh solutions in each laser excitation. All experiments were performed at 298 K.

ESR measurements: ESR spectra were recorded by using a JEOL JES-ME-LX X-band spectrometer at room temperature with photoirradiation from a USHIO USH1005D high-pressure mercury arc lamp (1000 W) equipped with a water filter to remove infrared light and a glass cutoff filter ($\lambda>340$ nm). Single crystals were used as a sample of each compound. ESR sample tubes (4.5 mm) charged with the samples were degassed and sealed under Ar. ESR measurements were performed under nonsaturating microwave power conditions. The amplitude of modulation was chosen to optimize the resolution and the signal-to-noise (*S*/*N*) ratio of the observed spectra. A Calleo ESR program[45] was used for simulations of ESR spectra to determine the hyperfine coupling constants.

TRESR measurements were carried out by using a JEOL JES-FE2XG EPR spectrometer at room temperature. Samples were excited by a Spectra Physics MOPO-710 OPO laser pumped with a Spectra Physics GCR-170-10 Nd/YAG laser at 585 nm. The TRESR signals from the ESR unit were integrated by a NF BX-531 boxcar integrator at 1 μs after the laser excitation.

Theoretical calculations: DFT calculations were performed on an 8CPU workstation (PQS, Quantum Cube QS8–2400C-064). Geometry optimizations were carried out by using the B3LYP functional and the 6-31G* basis set[46,47] with the unrestricted Hartree–Fock (UHF) formalism as implemented in the Gaussian 03 program.[48] Graphical outputs of the computational results were generated by using the GaussView software program (version 3.09).[49]

Acknowledgements

This work was supported by a grant from the Iketani Science and Technology Foundation and Grants-in-Aid (No. 18033033 for a Priority Area ("Chemistry of Coordination Space") and No. 17750039) from the Ministry of Education, Culture, Science, and Technology of Japan. We thank Dr. Masahiko Suenaga (Department of Chemistry, Kyushu University) for his help in performing ^{19}F NMR measurements. We also thank Prof. H. Kitagawa (Department of Chemistry, Kyushu University) for helpful discussions.

[1] J. R. Darwent, P. Douglas, A. Harriman, G. Porter, M.-C. Richoux, *Coord. Chem. Rev.* **1982**, *44*, 83–126.
[2] Z. Liu, H. Yan, K. Wang, T. Kuang, J. Zhang, L. Gui, X. An, W. Chang, *Nature* **2004**, *428*, 287–292.
[3] U. Ermler, G. Fritzsch, S. K. Buchanan, H. Michel, *Structure* **1994**, *2*, 925–936.
[4] F. Rappaport, M. Guergova-Kuras, P. J. Nixon, B. A. Diner, J. Lavergne, *Biochemistry* **2002**, *41*, 8518–8527.
[5] K. N. Ferreira, T. M. Iverson, K. Maghlaoui, J. Barber, S. Iwata, *Science* **2004**, *303*, 1831–1838.
[6] a) G. Steinberg-Yfrach, P. A. Liddell, S.-C. Hung, A. L. Moore, D. Gust, T. A. Moore, *Nature* **1997**, *385*, 239–241; b) G. Steinberg-Yfrach, J.-L. Rigaud, E. N. Durantini, A. L. Moore, D. Gust, T. A. Moore, *Nature* **1998**, *392*, 479–482; c) D. Gust, T. A. Moore, A. L. Moore, *Acc. Chem. Res.* **2001**, *34*, 40–48.
[7] a) R. Takahashi, Y. Kobuke, *J. Am. Chem. Soc.* **2003**, *125*, 2372–2373; b) Y. Kobuke, K. Ogawa, *Bull. Chem. Soc. Jpn.* **2003**, *76*, 689–708; c) D. Furutsu, A. Satake, Y. Kobuke, *Inorg. Chem.* **2005**, *44*, 4460–4462.
[8] a) E. K. L. Yeow, K. P. Ghiggino, J. N. H. Reek, M. J. Crossley, A. W. Bosman, A. P. H. J. Schenning, E. W. Meijer, *J. Phys. Chem. B* **2000**, *104*, 2596–2606; b) M.-S. Choi, T. Aida, T. Yamazaki, I. Yamazaki, *Angew. Chem.* **2001**, *113*, 3294–3298; *Angew. Chem. Int. Ed.* **2001**, *40*, 3194–3198; c) M.-S. Choi, T. Aida, T. Yamazaki, I. Yamazaki, *Chem. Eur. J.* **2002**, *8*, 2667–2678; d) M.-S. Choi, T. Aida, H. Luo, Y. Araki, O. Ito, *Angew. Chem.* **2003**, *115*, 4194–4197; *Angew. Chem. Int. Ed.* **2003**, *42*, 4060–4063.
[9] S. Fukuzumi, *Bull. Chem. Soc. Jpn.* **2006**, *79*, 177–195.
[10] a) A. D. Schwab, D. E. Smith, C. S. Rich, E. R. Young, W. F. Smith, J. C. de Paula, *J. Phys. Chem. B* **2003**, *107*, 11339–11345; b) A. D. Schwab, D. E. Smith, B. Bond-Watts, D. E. Johnston, J. Hone, A. T. Johnson, J. C. de Paula, W. F. Smith, *Nano Lett.* **2004**, *4*, 1261–1265; c) C. M. Drain, *Proc. Natl. Acad. Sci. USA* **2002**, *99*, 5178–5182.
[11] a) T. Hasobe, P. V. Kamat, V. Troiani, N. Solladié, T. K. Ahn, S. K. Kim, D. Kim, A. Kongkanand, S. Kuwabata, S. Fukuzumi, *J. Phys. Chem. B* **2005**, *109*, 19–23; b) T. Hasobe, S. Hattori, P. V. Kamat, S. Fukuzumi, *Tetrahedron* **2006**, *62*, 1937–1946.
[12] Z. Wang, C. Medforth, J. A. Shelnutt, *J. Am. Chem. Soc.* **2004**, *126*, 16720–16721.
[13] L.-L. Li, C.-J. Yang, W.-H. Chen, K.-J. Lin, *Angew. Chem.* **2003**, *115*, 1543–1546; *Angew. Chem. Int. Ed.* **2003**, *42*, 1505–1508; .
[14] a) M. E. Kosal, J.-H. Chou, S. R. Wilson, K. S. Suslick, *Nat. Mater.* **2002**, *1*,118–121; b) K. S. Suslick, P. Bhyrappa, J.-H. Chou, M. E. Kosal, S. Nakagaki, D. W. Smithenry, S. R. Wilson, *Acc. Chem. Res.* **2005**, *38*, 283–291.
[15] a) R. Harada, Y. Matsuda, H. Okawa, T. Kojima, *Angew. Chem.* **2004**, *116*, 1861–1864; *Angew. Chem. Int. Ed.* **2004**, *43*, 1825–1828; ; b) T. Kojima, R. Harada, T. Nakanishi, K. Kaneko, S. Fukuzumi, *Chem. Mater.* **2007**, *19*, 51–58.
[16] A preliminary report has appeared, see: R. Harada, T. Kojima, *Chem. Commun.* **2005**, 716–718.

[17] C.-J. Liu, W.-Y. Yu, S.-M. Peng, T. C. W. Mak, C.-M. Che, *J. Chem. Soc. Dalton trans.* **1998**, 1805–1812.
[18] D. J. Nurco, C. J. Medforth, T. P. Forsyth, M. M. Olmstead, K. M. Smith, *J. Am. Chem. Soc.* **1996**, *118*, 10918–10919.
[19] B. Ward, C. K. Chang, R. Young, *J. Am. Chem. Soc.* **1984**, *106*, 3943–3950.
[20] a) M. A. Castriciano, A. Romeo, V. Villari, N. Micali, L. M. Scolaro, *J. Phys. Chem. B* **2004**, *108*, 9054–9059; b) N. C. Maiti, S. Mazumdar, N. Periasamy, *J. Phys. Chem. B* **1998**, *102*, 1528–1538; c) D. C. Barber, R. A. Freitag-Beeston, D. G. Whitten, *J. Phys. Chem.* **1991**, *95*, 4074–4086.
[21] a) H. Kobayashi, *Curr. Opin. Solid State Mater. Sci.* **1997**, *2*, 440–445, and references therein; b) J. Frerraris, D. O. Cowan, V. Walatka, Jr., J. H. Perlstein, *J. Am. Chem. Soc.* **1973**, *95*, 948–949.
[22] C. R. Newman, C. D. Frisbie, D. A. da Silva Filho, J.-L. Brédas, P. C. Ewbank, K. R. Mann, *Chem. Mater.* **2004**, *16*, 4436–4451.
[23] AL for Windows98, Version 3.07, JEOL, Tokyo (Japan), **2002**.
[24] a) M. P. Bryn, C. J. Curtis, I. Goldberg, Y. Hsiou, S. I. Khan, P. A. Sawin, S. K. Tendick, C. E. Strouse, *J. Am. Chem. Soc.* **1991**, *113*, 6549–6557; b) M. P. Bryn, C. J. Curtis, Y. Hsiou, S. I. Khan, P. A. Sawin, S. K. Tendick, A. Terzis, C. E. Strouse, *J. Am. Chem. Soc.* **1993**, *115*, 9480–9497.
[25] I. Goldberg, *Chem. Eur. J.* **2000**, *6*, 3863–3870.
[26] For examples, see: a) K. Okamoto, S. Fukuzumi, *J. Phys. Chem. B* **2005**, *109*, 7713–7723; b) Y. Kashiwagi, K. Ohkubo, J. A. McDonald, I. M. Blake, M. J. Crossley, Y. Araki, O. Ito, H. Imahori, S. Fukuzumi, *Org. Lett.* **2003**, *5*, 2719–2721; c) D. M. Guldi, A. Hirsch, M. Scheloske, E. Dietel, A. Troisi, F. Zerbetto, M. Prato, *Chem. Eur. J.* **2003**, *9*, 4968–4979.
[27] a) K. Pattersson, K. Kilså, J. Mårtensson, B. Albinsson, *J. Am. Chem. Soc.* **2004**, *126*, 6710–6719; b) K. Ohkubo, P. J. Sintic, N. V. Tkachenko, H. Lemmetyinen, W. E, Z. Ou, J. Shao, K. M. Kadish, M. J. Crossley, S. Fukuzumi, *Chem. Phys.* **2006**, *326*, 3–14.
[28] We examined PET in PNC–H_2QF$_4$ and PNC–Cat under photoirradiation ($\lambda > 500$ nm) by using a 1000 W high-pressure Hg lamp equipped with a cutoff filter (Y-49; ASAHI TECHNOGLASS Corp., Japan). We confirmed that the same ESR signals as shown in Figure 6 were observed with the same hyperfine coupling constants.
[29] P. D. Sullivan, J. R. Bolton, W. E. Geiger, Jr., *J. Am. Chem. Soc.* **1970**, *92*, 4176–4180.
[30] W. T. Dixon, D. Murphy, *J. Chem. Soc. Faraday Trans. 2* **1976**, *72*, 1221–1230.
[31] J. Eloranta, M. Vuolle, *Magn. Reson. Chem.* **1998**, *36*, 98–103.
[32] M. C. Richoux, P. Neta, A. Harriman, S. Baral, P. Hambright, *J. Phys. Chem.* **1986**, *90*, 2462–2468.
[33] The SHACV method provides a superior approach to directly evaluating one-electron redox potentials in the presence of a follow-up chemical reaction relative to the more well-known dc and fundamental harmonic ac methods, see: a) M. R. Wasielewski, R. Breslow, *J. Am. Chem. Soc.* **1976**, *98*, 4222–4229; b) E. M. Arnett, K. Amarnath, N. G. Harvey, J. Cheng, *J. Am. Chem. Soc.* **1990**, *112*, 344–345; c) M. Patz, H. Mayr, J. Maruta, S. Fukuzumi, *Angew. Chem.* **1995**, *107*, 1351–1353; *Angew. Chem. Int. Ed. Engl.* **1995**, *34*, 1225–1227.
[34] A similar value was reported in toluene (1. 67 eV), see: J. L. Retsek, S. Gentemann, C. J. Medforth, K. M. Smith, V. S. Chirvony, J. Fajer, D. Holten, *J. Phys. Chem. B* **2000**, *104*, 6690–6693.
[35] The corresponding nanosecond laser flash photolysis could not be performed because the sample size required for the probe light of the nanosecond laser pulse was too large for samples in KBr pellets and the lowest laser power for nanosecond laser flash photolysis is still too high to avoid the destruction of KBr pellets.
[36] The bleaching at 720 nm in Figure 10a is attributed to the adsorption due to the Q band of H_4DPP^{2+}.
[37] G. N. R. Tripathi, *J. Am. Chem. Soc.* **1998**, *120*, 5134–5135.
[38] S. Yamauchi, *Bull. Chem. Soc. Jpn.* **2004**, *77*, 1255–1268.
[39] K. A. McLauchlan, *Modern Pulsed and Continuous-Wave Electron Spin Resonance*, Wiley, New York, **1990**, p. 285.
[40] *Chemically Induced Magnetic Polarization* (Eds.: L. T. Muss, P. W. Atkins, K. A. McLauchlan, J. B. Pederson), Reidel, Dordrecht, **1977**.
[41] H. Akahori, K. Morita, A. Nishijima, T. Mitsuhashi, K. Ohkubo, S. Fukuzumi, *J. Imaging Sci. Technol.* **2006**, *49*, 381–388.
[42] J. Fraxedas, *Molecular Organic Materials*, Cambridge University Press, Cambridge, **2006**.
[43] Crystal Structure, Version 3.7, Rigaku Corporation, Tokyo (Japan), **1998**.
[44] G. M. Sheldrick, SIR 97 and SHELX97, Programs for Crystal Structure Refinement, University of Göttingen, Göttingen (Germany), **1997**.
[45] Calleo ESR, Version 1.2, Calleo Scientific Software Publishers, Fort Collins CO, **1996**.
[46] a) A. D. Becke, *J. Chem. Phys.* **1993**, *98*, 5648; b) C. Lee, W. Yang, R. G. Parr, *Phys. Rev. B* **1998**, *37*, 785.
[47] W. J. Hehre, L. Radom, P. v. R. Schleyer, J. A. Pople, *Ab Initio Molecular Orbital Theory*, Wiley, New York, **1986**.
[48] Gaussian 03, Revision C.02, M. J. Frisch, G. W. Trucks, H. B. Schlegel, G. E. Scuseria, M. A. Robb, J. R. Cheeseman, J. A. Montgomery, Jr., T. Vreven, K. N. Kudin, J. C. Burant, J. M. Millam, S. S. Iyengar, J. Tomasi, V. Barone, B. Mennucci, M. Cossi, G. Scalmani, N. Rega, G. A. Petersson, H. Nakatsuji, M. Hada, M. Ehara, K. Toyota, R. Fukuda, J. Hasegawa, M. Ishida, T. Nakajima, Y. Honda, O. Kitao, H. Nakai, M. Klene, X. Li, J. E. Knox, H. P. Hratchian, J. B. Cross, V. Bakken, C. Adamo, J. Jaramillo, R. Gomperts, R. E. Stratmann, O. Yazyev, A. J. Austin, R. Cammi, C. Pomelli, J. W. Ochterski, P. Y. Ayala, K. Morokuma, G. A. Voth, P. Salvador, J. J. Dannenberg, V. G. Zakrzewski, S. Dapprich, A. D. Daniels, M. C. Strain, O. Farkas, D. K. Malick, A. D. Rabuck, K. Raghavachari, J. B. Foresman, J. V. Ortiz, Q. Cui, A. G. Baboul, S. Clifford, J. Cioslowski, B. B. Stefanov, G. Liu, A. Liashenko, P. Piskorz, I. Komaromi, R. L. Martin, D. J. Fox, T. Keith, M. A. Al-Laham, C. Y. Peng, A. Nanayakkara, M. Challacombe, P. M. W. Gill, B. Johnson, W. Chen, M. W. Wong, C. Gonzalez, J. A. Pople, Gaussian, Inc., Wallingford CT, **2004**
[49] GaussView, Version 3.09, R. Dennington II, T. Keith, J. Millam, K. Eppinnett, W. L. Hovell, R. Gilliland, Semichem, Inc., Shawnee mission KS, **2003**.

Received: November 17, 2006
Revised: June 8, 2007
Published online: July 30, 2007

